

# ANDA: A Novel Data Augmentation Technique Applied to Salient Object Detection

Daniel V. Ruiz, Bruno A. Krinski, and Eduardo Todt

Department of Informatics, Federal University of Paraná (UFPR), Curitiba, PR, Brazil

{dvruiz, bakrinski, todt}@inf.ufpr.br

**Abstract**—In this paper, we propose a novel data augmentation technique (ANDA) applied to the Salient Object Detection (SOD) context. Standard data augmentation techniques proposed in the literature, such as image cropping, rotation, flipping, and resizing, only generate variations of the existing examples, providing a limited generalization. Our method has the novelty of creating new images, by combining an object with a new background while retaining part of its salience in this new context; To do so, the ANDA technique relies on the linear combination between labeled salient objects and new backgrounds, generated by removing the original salient object in a process known as image inpainting. Our proposed technique allows for more precise control of the object’s position and size while preserving background information. Aiming to evaluate our proposed method, we trained multiple deep neural networks and compared the effect that our technique has in each one. We also compared our method with other data augmentation techniques. Our findings show that depending on the network improvement can be up to 14.1% in the F-measure and decay of up to 2.6% in the Mean Absolute Error.

## I. INTRODUCTION

Visual Saliency (or Visual Saliency) is the characteristic of some objects that makes them stand out from its surrounding regions and attract the attention of the human brain [1]. Light intensity, edge or line orientation, color, motion, and stereo disparity are examples of Visual Saliency features that attract human attention. It has a wide range of applications in Computer Vision and Image Processing, e.g., recognizing and tracking objects, image cropping and resizing, video and image compression and summarization [2], [3]. In robotics, it can be applied in a plethora of algorithms such as robot self-localization in unknown environments [4], find potential gas/odor sources [5] and as a visual cue for gaze shift as shown by [6], [7], [8].

The recent works in the Salient Object Detection (SOD) literature proposed the use of Deep Neural Networks to find the salient objects in images [9]. Besides the impressive results achieved, training deep learning methods requires vast amounts of data. The construction of large datasets is challenging, especially because of the manual labor demanded. To counter this issue, data augmentation is often applied to multiply the available labeled data. In the SOD field, data augmentation techniques are usually limited to image cropping and affine transformations. When relying purely on those operations, background information can be lost, and this lost data could be meaningful in segmentation learning.

In this paper, we propose a novel approach to data augmentation in the context of SOD. Our method uses a linear combination between a labeled salient object and a new background generated by removing the original salient object. This technique allows more precise control of the object’s position and size in the image while preserving the background information. The implementation of the method is publicly available<sup>1</sup>.

We present our findings on four distinct neural networks: three Fully Convolutional Networks (FCNs) with Residual Network (ResNet)-50, ResNet-101, and VGG-16 backbones, implemented on KittiSeg framework<sup>2</sup> [10], following Krinski *et. al* [11]; and the PoolNet<sup>3</sup> [12] with ResNet-50 backbone (a very recent network which achieved an impressive state of the art results in the SOD). The official code released by the authors of PoolNet was used in this work. We also compare our approach to other augmentation techniques proposed in the literature, such as horizontal flipping, rescale, rotation, and random cropping. Eight training sets were produced, as described in Section IV. For each network, cross-dataset tests were performed in eight different publicly available datasets. Each experiment repeated those tests varying only the training set.

## II. RELATED WORK

In this section, we briefly survey the data augmentation techniques used in recent SOD literature. Perazzi *et al.* [13] proposed a data augmentation based on an affine transformation of scale and translation. Transformation of scale is applied to generate objects with  $\pm 5\%$  of the original size and transformation of translation, shifting the objects with  $\pm 10\%$  from the original position. Thin-plate splines are also utilized to generate non-rigid deformations in the width and height of the salient objects. Bianco *et al.* [14] proposed a data augmentation based on random crop, where a square subfigure was chosen with a minimum size of 256 and up to the original size then resized to  $256 \times 256$ , random horizontal flip, and random change on luminance (gamma).

Aytekin *et al.* [15] generate five new images for each image in the training and validation sets with a super-pixel gridization method. Randomly flipping in the horizontal direction is another augmentation technique evaluated. Guo

<sup>1</sup><https://github.com/ruizvitor/ANDA>

<sup>2</sup><https://github.com/MarvinTeichmann/KittiSeg>

<sup>3</sup><https://github.com/backseason/PoolNet>

*et al.* [16] evaluated data augmentation techniques based on random rotation, horizontal and vertical shift, and horizontal and vertical flip on the ICOSEG [17] dataset. Liu *et al.* [12] also utilized a random horizontal flip to perform data augmentation. Huang *et al.* [18] proposed a data augmentation based on image crop. The bounding boxes of the salient objects are utilized to randomly sample five start and end positions in a way that the cropped images cover the entire salient object. They also applied augmentation techniques like horizontal flip in the cropped images, generating ten new samples per original training image. Similarly, Laroca *et al.* [19] exploited various data augmentation strategies, such as random flipping, rescaling, shearing, and cropping, to train their networks and avoid overfitting.

### III. PROPOSED WORK

In the first step of the ANDA method, all salient objects are removed from all images in the training dataset, in turn, generating a new background for each training image (details presented in Section III-A). The second step is the association of a salient object to a new background without objects inside (details presented in Section III-B). In order to preserve the saliency of the object when inserted into the new context, a proper background is chosen based on the technique described in Section III-C.

Changing the background of a salient object is not enough to further the generalization of the training dataset. So, an analysis of the position and size distribution of the labeled objects on multiple datasets used in the SOD literature was performed, see Fig. 2. After analyzing the position distribution, a lack of samples closer to the margins was also observed, see Fig. 2a. A concentration in the proportional size of the object to the entire image was observed on the MSRA10K dataset [20], see Fig. 2b. Those distributions undermine its generalization, so to produce new samples that are diverse in size and position, affine transformations were used in the labeled objects before associating objects in a new background. Further details are presented in Section III-D.

#### A. Background Image Generation

Part of the novelty of this method is the use of a technique called image inpainting, which is the process of restoring missing pixels in digital images in a plausible way. Research in image inpainting has received considerable attention in different areas, such as restoration of old and damaged documents, removal of unwanted objects, and retouching applications [21]. More specifically, we use the neural network architecture named PConv proposed by Liu *et al.* [22]. The PConv is a UNet-like architecture [23] and was used in our work to remove the labeled salient object of each image of the MSRA10K dataset, creating background only images. In this work, a variation of an unofficial implementation was used with pre-trained weights from ImageNet [24], an example of full remotion is shown in Fig. 1.

#### B. Linear Combination of object and background

When combining an object  $o$  with and background only image  $b$ ,  $o$  and  $b$  are padded, ensuring that both have the

same width and height. The ground-truth mask  $m_o$  (composed by zeros and ones, where one is a salient pixel) of the object  $o$ , is dilated using a  $3 \times 3$  kernel and mean blurred using a  $3 \times 3$  kernel to achieve a smooth transition between the object and the background. The  $\alpha$  transparency of the object is changed by multiplying  $m_o$  by 0.95. The resulting image  $r$  is cropped to  $b$  original width and height.

#### C. Background Choosing

When a salient object is inserted in a new background, the salient object may no longer be salient. In order to choose a background which maintains the object's saliency, we compute a feature vector of 256 positions composed of four histograms (64 bins for Hue, 64 for Saturation, 64 for Value, and 64 for Local Binary Patterns (LBP) [25], with the parameters: number of circularly symmetric neighbour set points: 24, circle radius: 3, and method: uniform) for the salient object and the new background.

A K-Nearest Neighbors (kNN) with  $k = 10,000$  (10,000 is the number of images in the MSRA10K dataset) is computed using the cosine similarity defined at Equation 1. The similarity value is obtained by using the feature vector  $A$  (the salient object without its original background) and the feature vector  $B$  (new background image). In this way  $d_c(A, B)$  shows the similarity between the object and the background.

$$d_c(A, B) = \frac{\sum_{j=1}^N A_j B_j}{\sqrt{\sum_{j=1}^N A_j^2} \sqrt{\sum_{j=1}^N B_j^2}} \quad (1)$$

The  $\lfloor \frac{k}{2} \rfloor$ th nearest neighbor was chosen to preserve the saliency of the generated image. This particular value was adopted since the images with higher values are very different, while those with lower values are very similar, in this way a middle ground between those extremes seems to be the best choice, producing images that are closer to the real-world samples. In Section IV, three experiments were performed to evaluate this assumption.

#### D. Size and Position Distribution

The position and size distribution of the objects in the datasets were evaluated as follows. For each image, is generated the bounding box containing all objects inside the image. The position distribution analysis can be observed in a scatter plot where the center coordinates of the bounding box (normalized) are used, with a heat colormap for sample density, as shown in Fig. 2a. The size distribution analysis can be observed in a ten bin histogram, where the area of the bounding box is divided by the area of the image to obtain the proportion of the bounding box over the entire image, as shown in Fig. 2b.

Since the MSRA10K dataset is the training dataset, the goal is to generate new samples with a high variation of position and size, approximating the distribution of the dataset to a uniform distribution. Since in this dataset there is a concentration of samples in the  $[0.2, 0.3)$ ,  $[0.3, 0.4)$ ,  $[0.4, 0.5)$  intervals, new samples don't need to be produced in those

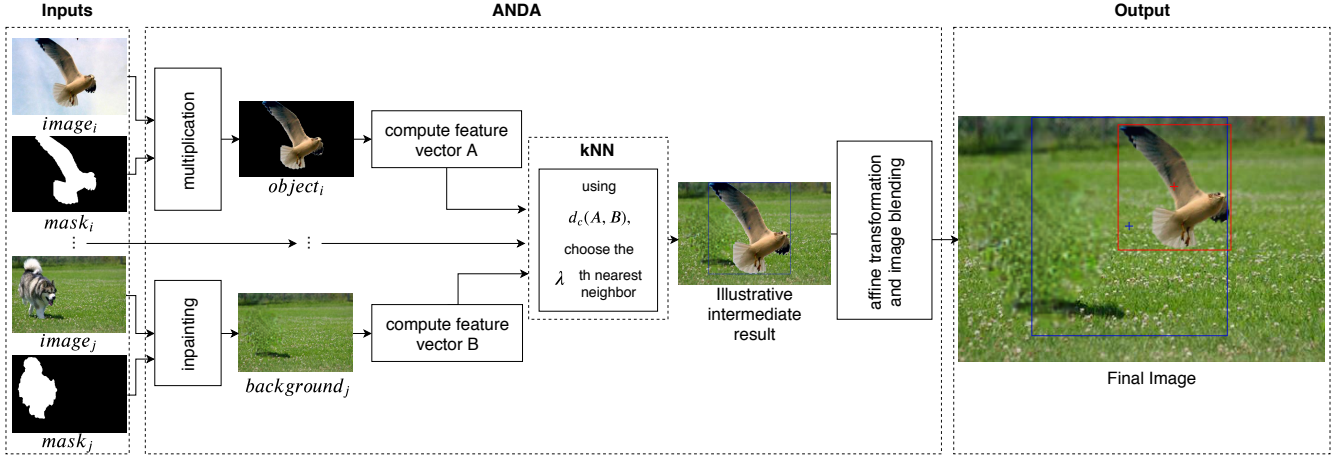


Fig. 1. Overview diagram of the ANDA technique. The first step is the computation of a background image for all the images of the inputted dataset, an object image is also computed; those images are used to produce feature vectors that can be compared using kNN with cosine similarity;  $\lambda$  stands for the criteria chosen. Three different criteria were evaluated, see Section IV. Finally, for each pair of  $object_i$  and  $background_{\lambda}$ , a final image is created using a linear combination of both. Note that in  $mask_j$  the dog's shadow is not included, so  $background_j$  preserve this information. In the final image and the intermediate result, blue represents the original bounding box; red represents the bounding box after an affine transformation; the crosses represent the respective center of the bounding boxes.

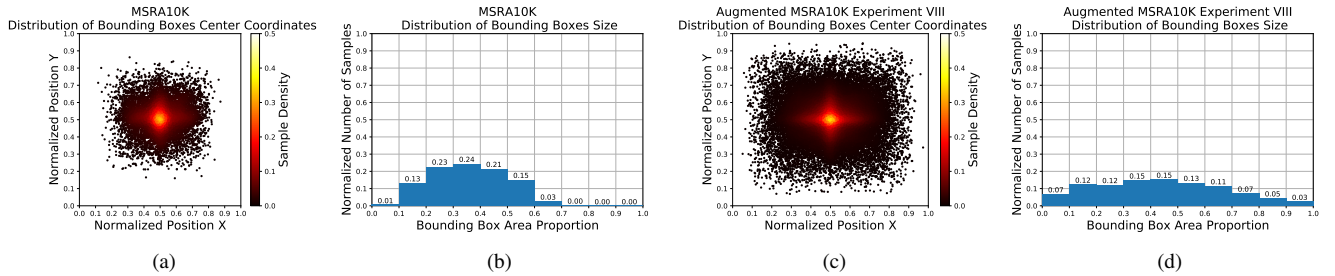


Fig. 2. Position and size distributions per dataset. For position, the normalized bounding box center coordinates and heat colormap for sample position density, are presented as a scatter plot. For size, the bounding box area divided by image area is displayed in a 10-bin histogram. Figs 2a, 2b correspond to the MSRA10K, the dataset used for training, and Figs 2c, 2d correspond to the augmented MSRA10K as defined by experiment VIII, see Section IV for further details.

scales, neither in the  $[0.9, 1.0]$  interval, since an object in this size range, is not as useful for training, because it almost completely occlude the background. Since there is already a concentration on the center, for the position, the goal is to approximate the new samples to the margins, causing a dispersion on the samples.

The training dataset is composed of  $k$  images. The index  $i$  represents the  $i$ th image inside the training dataset. Each image  $i$  has an object  $o$ , a background  $b$ , and a bounding box  $\phi$  defined by two corner points  $v = (x_{\min}, y_{\min}) = (x, y)$  and  $v' = (x_{\max}, y_{\max}) = (x', y')$ . The bounding box has a width  $w_{\phi} = x' - x$ , a height  $h_{\phi} = y' - y$ , and an area  $a_{\phi} = w_{\phi} * h_{\phi}$ . The background has a width  $w_b$ , a height  $h_b$ , and an area  $a_b = w_b * h_b$ .

Aiming to resize the object  $o$ , we multiply its width and height to a scale factor  $s$ , if the resized object  $o'$  can fit  $b$  then  $s$  is defined as in Equation 2 otherwise as in Equation 5, generating a new object  $o'$  with  $w'_o = w_o * s$  and  $h'_o = h_o * s$ .

$$s = \sqrt{\frac{p \times a_b}{a_{\phi}}} \quad (2)$$

If the resized object  $o'$  fits  $b$ ,  $s$  is as defined by Equation 2, where  $p$  (Equation 3) is a scale factor to increase the number of objects with that given scale.  $\beta$  defined at Equation 4 is a vector of scales, defined based on the lack of objects in those scales in the original dataset, as pointed out previously, and  $\gamma$  is a vector of random values in the interval  $[0.975, 1.025]$  following a uniform distribution. The values in  $\gamma$  are noises to generate objects close to the desired size, but not exactly as defined in  $\beta$ , increasing the diversity of object sizes.

$$p = \beta_{(i \bmod 5)} \times \gamma_i \quad (3)$$

$$\beta = [0.05 \quad 0.15 \quad 0.65 \quad 0.75 \quad 0.85]^T \quad (4)$$

$$s = \min\left(\frac{w_b}{x' - x}, \frac{h_b}{y' - y}\right) \quad (5)$$

Otherwise, if the resized object  $o'$  cannot fit  $b$ , there are two cases, first case: both  $\phi$  and  $b$  have the same orientation, landscape or portrait, then  $s$  is defined as in Equation 5, i.e.,  $s$  receives the highest possible value to resize the object without deforming it or overflowing the background. The second case,  $\phi$ , and  $b$  have a different orientation, then  $o$  is rotated by  $-90^\circ$  degrees or  $90^\circ$  degrees, the sign of the value is chosen based on a random binary value, then the same resize as the first case occurs.

To disperse the objects center position in the dataset a translation is performed on  $o$ , in such a way that  $\phi'$  still in the boundaries of  $b$ , if there is free space in both directions for each axis. A random binary value decides the direction, the remaining space between  $\phi'$  and the boundary is then multiplied by  $\theta_{rx}$  and  $\theta_{ry}$  which are vectors of random values in the interval  $[0.0, 1.0]$  following a uniform distribution. An example of the effect of doing those operations is displayed in Fig. 1.

#### IV. EXPERIMENTS

In order to evaluate the network models, we utilize nine datasets of salient objects widely used in the SOD literature: DUT-OMRON [26], ECSSD [27], HKU-IS [28], ICOSEG [17], MSRA10K [20], PASCAL-S [29], SED1 [30], SED2 [30], and THUR [31].

The datasets are composed by images containing salient objects with different biases (*e.g.*, number of salient objects, image clutter, center-bias) and the referent ground truth mask with the expected segmentation of the salient objects. The ground truth masks are binary images with the salient regions in white (value 255) and the background with no salient regions in black (value 0).

##### A. Evaluation Metrics

The architecture models trained in the SOD problem are evaluated and compared through four metrics widely used in the SOD literature: Precision, Recall, F-measure also known as F-score, and Mean Absolute Error (MAE). The  $\beta$  in the F-measure formula changes the Precision and Recall importance. In the SOD literature,  $\beta^2$  receives the value 0.3 [30], [32] to increase the Precision importance.

##### B. Experiments

We present our findings on four distinct neural networks. Three FCNs with ResNet-50, ResNet-101 and VGG-16 backbones, implemented on KittiSeg framework [10] and the PoolNet [12] with ResNet-50 backbone. We also compare our approach to other augmentation techniques proposed in the literature, such as horizontal flipping, rescale, rotation and random cropping.

The FCNs with ResNets 50 and 101 backbones were trained with 40,000 and 60,000 iterations respectively, receiving an initial learning rate of  $10^{-6}$ . We also utilized an exponential learning rate decay, similar with the proposed in the literature [33], and the initial learning rate is divided by 10 at the 50,000th iteration. The FCN with VGG-16 backbone was trained with 100,000 iterations, receiving an

initial learning rate of  $10^{-5}$  which is divided by 10 at the 50,000th iteration, generating a learning rate which is divided by 10 at the 75,000th.

All the PoolNet experiments are performed using a weight decay of  $5 \times 10^{-4}$  and an initial learning rate of  $5 \times 10^{-5}$  which is divided by 10 after 15 epochs (with an epoch been  $n$  iterations, with  $n$  the number of images on the training dataset). Thus, each PoolNet experiment were trained for 24 epochs in total, both the baseline and the data-augmented ones were trained with the same number of epochs. Joint Training with Edge Detection was not performed.

In the first step, all networks were trained in the MSRA10K dataset (baseline) without any alteration. Then, we generated eight new training sets with augmentation applied in the MSRA10K images:

- (I) MSRA10K + horizontal flip (20,000 images in total).
- (II) MSRA10K + uniformly distributed random rotations between  $[-30^\circ, 30^\circ]$  (20,000).
- (III) MSRA10K + uniformly distributed random resizes between  $[0.9, 1.1]$  (20,000).
- (IV) MSRA10K + uniformly distributed random crop preserving the salient object (20,000).
- (V) MSRA10K + ANDA technique limiting the distance between the object and the background to less than 0.1, considering the cosine similarity as previously discussed in Section III-C (20,000).
- (VI) MSRA10K + ANDA technique limiting the distance between the object and the background to greater than 0.25 (20,000).
- (VII) MSRA10K + ANDA technique taking the background with  $\lfloor \frac{k}{2} \rfloor$ th nearest neighbor (20,000).
- (VIII) In this experiment, let  $\Omega$  be the union set of the augmentation IV and VII, and  $\omega$  a uniformly distributed random selection of 15,000 images from  $\Omega$ . In  $\omega$  was performed horizontal flip, a uniformly distributed random rescale of  $[0.9, 1.1]$ , and uniformly distributed random rotation of  $[-30^\circ, 30^\circ]$ . The Experiment VIII is composed of MSRA10K +  $\Omega$  +  $\omega$  (45,000 images in total).

#### V. DISCUSSION

To ensure a fair comparison between our proposed approach and the commonly used techniques on the literature, we isolate each technique, defined the parameters, further details in Section IV, and compared one another on the same network.

In Table I we present the results achieved with the baseline (MSRA10K), and in the eight augmentations performed in our work in the FCN with ResNet-50 backbone. The proposed augmentation ANDA achieved the highest F-measure in the DUT-OMRON, SED1, SED2, and achieved the highest Precision in all datasets, with exception of the ICOSEG. In the last augmentation (VIII), where we combined the proposed ANDA with other augmentation techniques, we achieved the highest F-measures in seven of eight datasets and achieved the smallest MAE in three of eight datasets. Experiment VII outperformed V and VI in all datasets when

TABLE I

COMPARISON BETWEEN BASELINE AND DATA AUGMENTED RESULTS. BEST F-SCORE, PRECISION, AND MAE PER DATASET ARE HIGHLIGHTED IN BLUE, RED, AND ORANGE RESPECTIVELY. DUT-O\* IS AN ABBREVIATION OF DUT-OMRON.

Experiment	Metric	DUT-O*	ECSSD	HKU-IS	ICOSEG	PASCAL-S	SED1	SED2	THUR
Baseline	F-score	0.499	0.790	0.761	0.748	0.714	0.641	0.408	0.617
	Precision	0.681	0.887	0.870	0.826	0.823	0.890	0.848	0.691
	Recall	0.441	0.697	0.665	0.692	0.646	0.497	0.264	0.649
	MAE	0.106	0.092	0.073	0.087	0.104	0.129	0.148	0.099
(I) H-Flip [12], [14], [15], [16], [18], [19]	F-score	0.499	0.798	0.762	0.760	0.717	0.664	0.386	0.610
	Precision	0.661	0.875	0.854	0.821	0.808	0.885	0.780	0.670
	Recall	0.444	0.729	0.691	0.719	0.672	0.542	0.258	0.660
	MAE	0.102	0.085	0.071	0.081	0.100	0.120	0.148	0.101
(II) Rotate [16], [19]	F-score	0.513	0.799	0.789	0.745	0.726	0.645	0.481	0.651
	Precision	0.689	0.882	0.858	0.804	0.825	0.888	0.860	0.690
	Recall	0.461	0.723	0.733	0.746	0.669	0.521	0.336	0.722
	MAE	0.105	0.090	0.066	0.090	0.101	0.131	0.138	0.095
(III) Resize [13], [19]	F-score	0.504	0.799	0.770	0.765	0.721	0.644	0.411	0.611
	Precision	0.689	0.887	0.867	0.840	0.825	0.888	0.875	0.694
	Recall	0.437	0.717	0.685	0.704	0.659	0.514	0.266	0.641
	MAE	0.102	0.087	0.069	0.081	0.102	0.125	0.143	0.100
(IV) Crop [14], [18], [19]	F-score	0.523	0.800	0.779	0.739	0.726	0.641	0.409	0.625
	Precision	0.687	0.890	0.873	0.826	0.830	0.870	0.880	0.692
	Recall	0.473	0.710	0.691	0.667	0.656	0.505	0.271	0.659
	MAE	0.104	0.089	0.069	0.087	0.102	0.129	0.144	0.097
(V) ANDA $\leq 0.1$	F-score	0.517	0.798	0.790	0.753	0.715	0.622	0.480	0.646
	Precision	0.713	0.899	0.887	0.832	0.848	0.916	0.865	0.709
	Recall	0.437	0.695	0.686	0.692	0.617	0.483	0.338	0.681
	MAE	0.104	0.096	0.072	0.099	0.109	0.141	0.142	0.096
(VI) ANDA $\geq 0.25$	F-score	0.530	0.787	0.768	0.755	0.707	0.651	0.478	0.624
	Precision	0.702	0.899	0.885	0.836	0.849	0.920	0.907	0.702
	Recall	0.469	0.666	0.650	0.698	0.599	0.485	0.309	0.627
	MAE	0.101	0.098	0.076	0.098	0.112	0.135	0.144	0.099
(VII) ANDA $\lfloor \frac{k}{2} \rfloor$ th neighbor	F-score	0.530	0.799	0.788	0.755	0.717	0.683	0.473	0.646
	Precision	0.707	0.901	0.881	0.823	0.844	0.924	0.877	0.706
	Recall	0.462	0.697	0.697	0.723	0.628	0.545	0.337	0.682
	MAE	0.100	0.093	0.070	0.093	0.107	0.130	0.142	0.095
(VIII)	F-score	0.549	0.813	0.803	0.758	0.730	0.694	0.549	0.659
	Precision	0.700	0.885	0.867	0.811	0.838	0.917	0.885	0.688
	Recall	0.496	0.734	0.739	0.739	0.658	0.573	0.382	0.737
	MAE	0.103	0.089	0.066	0.092	0.105	0.124	0.133	0.095

TABLE II

COMPARISON BETWEEN BASELINE AND DATA AUGMENTED RESULTS. BEST F-SCORE AND MAE PER NETWORK ARE HIGHLIGHTED IN BOLD TEXT. DUT-O\* IS AN ABBREVIATION OF DUT-OMRON.

Network	Experiment	Metric	DUT-O*	ECSSD	HKU-IS	ICOSEG	PASCAL-S	SED1	SED2	THUR	
FCN ResNet-101	Baseline	F-score	0.442	0.766	0.735	0.682	0.691	0.538	0.315	0.576	
		MAE	0.107	0.094	0.075	0.108	0.107	0.152	0.186	0.102	
	VII	F-score	0.440	0.761	0.731	0.643	0.657	0.439	0.314	0.586	
		MAE	0.104	0.103	0.082	0.124	0.123	0.170	0.164	0.097	
	VIII	F-score	0.469	0.784	0.771	0.696	0.685	0.490	0.345	0.620	
		MAE	0.101	0.096	0.072	0.112	0.114	0.161	0.160	0.094	
	VGG-16	Baseline	F-score	0.695	0.863	0.840	0.806	0.797	0.858	0.590	0.722
			MAE	0.067	0.081	0.064	0.094	0.092	0.079	0.134	0.074
VII		F-score	0.664	0.850	0.839	0.793	0.777	0.823	0.616	0.710	
		MAE	0.078	0.084	0.066	0.096	0.099	0.086	0.134	0.078	
VIII		F-score	0.687	0.857	0.844	0.799	0.788	0.848	0.647	0.719	
		MAE	0.070	0.081	0.065	0.092	0.095	0.080	0.125	0.075	
PoolNet ResNet-50		Baseline	F-score	0.737	0.903	0.893	0.844	0.844	0.906	0.815	0.726
			MAE	0.060	0.049	0.036	0.071	0.068	0.047	0.085	0.073
	VII	F-score	0.735	0.901	0.889	0.831	0.839	0.912	0.814	0.721	
		MAE	0.066	0.048	0.037	0.071	0.070	0.045	0.077	0.075	
	VIII	F-score	0.725	0.904	0.884	0.829	0.837	0.915	0.845	0.717	
		MAE	0.072	0.046	0.038	0.070	0.070	0.041	0.068	0.078	

evaluating the MAE encouraging our previous assumption of Section III-C.

In Table II we present a comparison of three networks, a FCN with ResNet-101 backbone, a FCN with VGG-16 backbone and PoolNet with ResNet-50 backbone. The three networks were trained with three training sets: the MSRA10K (baseline), our proposed ANDA (augmentation VII), and our proposed ANDA with other augmentation techniques (VIII). With the FCN with ResNet-101 backbone, the augmentation VIII achieved the highest F-measure in six of eight datasets, and achieved the smallest MAE in four datasets. Our method was not so effective with the FCN with VGG-16 backbone, and improved the F-measure only in two datasets, when compared with the same network trained with the baseline. Finally, with the PoolNet, the augmentation VIII achieved higher F-measure in three datasets, and achieved better MAE in four datasets.

## VI. CONCLUSION

In this work, we proposed a novel data augmentation technique (ANDA) for the Visual Saliency problem and performed experiments on eight different training sets, where the combination of diverse data augmentation techniques widely utilized in the SOD literature and our technique are compared. For each network, cross-dataset tests were performed in eight different publicly available datasets. Each experiment repeated those tests varying only the training set. The experiments have shown that the ANDA technique when combined with other conventional approaches, such as random cropping, horizontal flipping, rotation, and re-scale, provides improvements even in the PoolNet, a very recent state of the art network. Further exploration of this technique on other networks and contexts was left for future works.

## ACKNOWLEDGMENT

The authors would like to thank the Coordination for the Improvement of Higher Education Personnel (CAPES) for the Masters scholarship. We gratefully acknowledge the founders of the publicly available datasets and the support of NVIDIA Corporation with the donation of the GPUs used for this research.

## REFERENCES

- [1] L. Itti, C. Koch, and E. Niebur, "A model of saliency-based visual attention for rapid scene analysis," *IEEE Transactions on Pattern Analysis and Machine Intelligence*, vol. 20, no. 11, pp. 1254–1259, Nov 1998.
- [2] G. Lee, Y. Tai, and J. Kim, "Deep saliency with encoded low level distance map and high level features," in *IEEE Conference on Computer Vision and Pattern Recognition (CVPR)*. IEEE, June 2016.
- [3] X. Xi, Y. Luo, F. Li, P. Wang, and H. Qiao, "A fast and compact saliency score regression network based on fully convolutional network," *CoRR*, vol. abs/1702.00615, 2017.
- [4] E. Todt and C. Torras, "Outdoor landmark-view recognition based on bipartite-graph matching and logistic regression," in *IEEE International Conference on Robotics and Automation*, 2007, pp. 4289–4294.
- [5] H. Ishida, H. Tanaka, H. Taniguchi, and T. Moriizumi, "Mobile robot navigation using vision and olfaction to search for a gas/odor source," *Autonomous Robots*, vol. 20, no. 3, pp. 231–238, Jun 2006.
- [6] F. Orabona, G. Metta, and G. Sandini, "Object-based visual attention: a model for a behaving robot," in *CVPR - Workshops*, Sep. 2005.
- [7] N. Kirchner, A. Alempijevic, and G. Dissanayake, "Nonverbal robot-group interaction using an imitated gaze cue," in *International Conference on Human-robot Interaction*. ACM, 2011, pp. 497–504.
- [8] A. P. Shon *et al.*, "Probabilistic gaze imitation and saliency learning in a robotic head," in *IEEE International Conference on Robotics and Automation*, 2005, pp. 2865–2870.
- [9] A. Borji, M.-M. Cheng, H. Jiang, and J. Li, "Salient object detection: A survey," *CoRR*, vol. abs/1411.5878, 2014.
- [10] M. Teichmann, M. Weber, J. M. Zöllner, R. Cipolla, and R. Urtasun, "Multinet: Real-time joint semantic reasoning for autonomous driving," *IEEE Intelligent Vehicles Symposium*, pp. 1013–1020, 2018.
- [11] B. A. Krinski, D. V. Ruiz, G. Z. Machado, and E. Todt, "Masking salient object detection, a mask region-based convolutional neural network analysis for segmentation of salient objects," *arXiv preprint*, vol. arXiv:1909.08038, pp. 1–6, 2019.
- [12] J.-J. Liu, Q. Hou, M.-M. Cheng, J. Feng, and J. Jiang, "A simple pooling-based design for real-time salient object detection," in *CVPR*. IEEE, 2019.
- [13] F. Perazzi *et al.*, "Learning video object segmentation from static images," in *CVPR*. IEEE, 2017.
- [14] S. Bianco, M. Buzzelli, and R. Schettini, "A fully convolutional network for salient object detection," in *Image Analysis and Processing - ICIAP*, 2017, pp. 82–92.
- [15] C. Aytekin, X. Ni, F. Cricri, L. Fan, and E. Aksu, "Memory-efficient deep salient object segmentation networks on gridized superpixels," in *IEEE International Workshop on Multimedia Signal Processing (MMSP)*, Aug 2018, pp. 1–6.
- [16] L. Guo and S. Qin, "High precision detection of salient objects based on deep convolutional networks with proper combinations of shallow and deep connections," *Symmetry*, vol. 11, no. 1, 2018.
- [17] D. Batra, A. Kowdle, D. Parikh, J. Luo, and T. Chen, "iCoseg: Interactive co-segmentation with intelligent scribble guidance," in *CVPR*. IEEE, 2010, pp. 3169–3176.
- [18] R. Huang, Y. Xing, and Z. Wang, "Rgb-d salient object detection by a cnn with multiple layers fusion," *IEEE Signal Processing Letters*, vol. 26, no. 4, pp. 552–556, April 2019.
- [19] R. Laroca, L. A. Zanlorensi, G. R. Gonçalves, E. Todt, W. R. Schwartz, and D. Menotti, "An efficient and layout-independent automatic license plate recognition system based on the YOLO detector," *arXiv preprint*, vol. arXiv:1909.01754, pp. 1–14, 2019.
- [20] M.-M. Cheng, N. J. Mitra, X. Huang, P. H. S. Torr, and S.-M. Hu, "Global contrast based salient region detection," *IEEE TPAMI*, vol. 37, no. 3, pp. 569–582, 2015.
- [21] M. A. Qureshi, M. Deriche, A. Beghdadi, and A. Amin, "A critical survey of state-of-the-art image inpainting quality assessment metrics," *Journal of Visual Communication and Image Representation*, vol. 49, pp. 177 – 191, 2017.
- [22] G. Liu, F. A. Reda, K. J. Shih, T.-C. Wang, A. Tao, and B. Catanzaro, "Image inpainting for irregular holes using partial convolutions," in *Computer Vision (ECCV)*, 2018, pp. 89–105.
- [23] O. Ronneberger, P. Fischer, and T. Brox, "U-net: Convolutional networks for biomedical image segmentation," in *Medical Image Computing and Computer-Assisted Intervention*, 2015, pp. 234–241.
- [24] J. Deng, W. Dong, R. Socher, L.-J. Li, K. Li, and L. Fei-Fei, "ImageNet: A Large-Scale Hierarchical Image Database," in *CVPR*, 2009.
- [25] T. Ojala, M. Pietikainen, and T. Maenpaa, "Multiresolution gray-scale and rotation invariant texture classification with local binary patterns," *IEEE Transactions on Pattern Analysis and Machine Intelligence*, vol. 24, no. 7, pp. 971–987, July 2002.
- [26] C. Yang, L. Zhang, R. X. Lu, Huchuan, and M.-H. Yang, "Saliency detection via graph-based manifold ranking," in *CVPR*. IEEE, 2013.
- [27] J. Shi, Q. Yan, L. Xu, and J. Jia, "Hierarchical image saliency detection on extended cssd," *IEEE Transactions on Pattern Analysis and Machine Intelligence*, vol. 38, no. 4, pp. 717–729, April 2016.
- [28] G. Li and Y. Yu, "Visual saliency based on multiscale deep features," *CVPR*, pp. 5455–5463, 2015.
- [29] Y. Li, X. Hou, C. Koch, J. M. Rehg, and A. L. Yuille, "The secrets of salient object segmentation," *CVPR*, pp. 280–287, 2014.
- [30] A. Borji, M.-M. Cheng, H. Jiang, and J. Li, "Salient object detection: A benchmark," *IEEE TIP*, vol. 24, no. 12, pp. 5706–5722, 2015.
- [31] M.-M. Cheng, N. Mitra, X. Huang, and S.-M. Hu, "Salientshape: group saliency in image collections," *The Visual Computer*, vol. 30, no. 4, pp. 443–453, 2014.
- [32] R. Achanta, S. Hemami, F. Estrada, and S. Susstrunk, "Frequency-tuned salient region detection," in *CVPR*, June 2009, pp. 1597–1604.
- [33] M. Z. Alom *et al.*, "The history began from alexnet: A comprehensive survey on deep learning approaches," *CoRR*, 2018.